JOURNAL OF MATERIALS SCIENCE 29 (1994) 1310–1318

Fibre stress and strain in fibre-reinforced composites

R. M. ASPDEN
Department of Orthopaedics, University of Aberdeen, Aberdeen AB9 2ZD, UK

Stress is transferred to the fibres in a fibrous composite material through interactions at the fibre surface. A number of descriptions of different transfer processes have been developed but these give little information on the state of stress within the fibre itself. The analysis presented here enables the internal stresses and strains generated within the fibre by the different stress transfer mechanisms to be analysed. The results show clearly different stress patterns for the mechanisms studied; fibres in a plastic or metallic matrix compared with those in an elastic matrix. The definition of a 'critical length' in the latter case is not so clear as is sometimes suggested.

1. Introduction

Fibrous composite materials have recently gained great technological importance owing to their superior performance and versatility. Embedding stiff fibres in a softer matrix can lead to some outstanding mechanical properties, including the advantages of both fibre and matrix, such as high strength and large elongation to fracture. Biological systems have been using composites from before recorded history and they form the vast majority of supporting tissues in both the plant and animal kingdoms. Such materials have developed to fulfil many mechanical functions, ranging from those permitting only small displacements, e.g. wood or bone, to tissues which have developed mechanisms for reorienting fibres and which can safely withstand strains of approaching 100% [1].

The mechanisms of stress-transfer from the matrix to the, generally stronger and stiffer, fibres are slowly being elucidated from both theoretical and experimental approaches [2–7]. These enable the calculation of stress-transfer lengths, commonly known as critical lengths, and are obviously of prime importance. While these studies generally make clear exactly the system that is being studied, popularized versions or summaries of results in books [8, 9] often seem to confuse the elastic analyses, such as those by Cox [2], with those derived for metals and polymers which rely on either a plastic or a frictional transfer of stress [3]. Although the mean axial stress within a fibre can be estimated, no method has yet been proposed to calculate the distribution of the various stresses and strains within the fibres themselves. Such analysis would not only calculate internal stresses and strains generated within the fibre but would also demonstrate clearly the different stress distributions to be expected from the various models for stress transfer.

This paper attempts to address this problem by presenting an analytical method for calculating the stresses and strains within a fibre from a given stress distribution at the surface represented by a Fourier series. To simplify the analysis, the fibre is assumed to be isotropic and homogeneous and only stresses over the curved, cylindrical surface are considered here. First the general equation to be solved is set up for stresses and displacements within the fibre. Then the general solution is derived for the case of stresses at the curved surface of the fibre before analysing a number of examples of different shear stress distributions only. However, these restrictions can be lifted in future studies to include normal stresses both at the fibre ends and radially directed. The solutions obtained will be put into the context of different fibre–matrix combinations in which these stresses could arise.

2. Method

The method adopted is to obtain symmetrical solutions to the equations of elasticity in cylindrical coordinates [10]. A rigorous derivation has been performed previously [11] and the results derived here are based largely on that analysis. An outline of the derivation is given in Appendix A for completeness and accessibility, but for a rigorous analysis, one is referred to Filon's original paper. A cylindrical polar coordinate system is used throughout the analysis. The fibre has a radius a and length $2c$ but because of symmetry only a half-fibre $0 \leqslant z \leqslant c$ needs to be considered. Its material properties are assumed to be isotropic and homogeneous and can therefore be represented by the Lamé constants, λ and μ. Though λ does not have the same clear physical interpretation as other material parameters, its use does simplify the writing of the equations and it will be seen that formulae can be derived that allow ready alteration of model parameters such as Poisson's ratio. Let σ_{xy} denote the stress parallel to dx across an element of surface perpendicular to dy where x and y can stand for any of r, φ, z. Also, let u, v, w denote the radial, circumferential and longitudinal displacements, respectively, in the fibre. Solutions are required to a fourth-order differential equation of the form

$$\nabla^2 \nabla^2 f = 0 \quad (1)$$

0022–2461

where ∇ is Laplace's operator in cylindrical polar coordinates and f may stand for either du/dz or dw/dr [11]. The required solutions for this system, which are in the form of a combination of trigonometric and Bessel's functions, are outlined in Appendix A. It may be seen that the solutions for radial and longitudinal displacements are independent of those for transverse displacements and that, similarly, the stresses $\sigma_{\varphi z}$ and $\sigma_{r\varphi}$, which would generate torsion in the fibre, depend only on v and are thus independent of the other stresses.

For the purposes of this analysis, only stresses at the cylindrical surface of the fibre will be considered. In this case, the normal stress, σ_{zz}, over the faces $z = \pm c$ is identically zero. The radial stress is described by an even function of z over the surface $r = a$ and is given by $\sigma_{rr} = \mu f(z)$, and the shear stress is an odd function over the curved surface $r = a$ and is given by $\sigma_{rz} = \mu g(z)$. These attributes are often overlooked, but arise from symmetry considerations and, for the shear stress, the requirement for equilibrium; a fibre must be pulled equally but in opposite directions at any corresponding points either side of the central origin. Applied stresses are normalized by the fibre shear modulus to make the results independent of the particular fibre. No account is taken of the surrounding matrix other than that it can generate the stresses described by $f(z)$ and $g(z)$.

The functions $f(z)$ and $g(z)$ can be expanded in the form of Fourier series between the limits $z = \pm c$ in the form

$$f(z) - f(c) = \sum_{n=0}^{\infty} a_n \cos[(2n+1)\pi z/2c] \quad (2a)$$

$$a_n = \frac{1}{c}\int_{-c}^{+c} [f(z) - f(c)]\cos[(2n+1)\pi z/2c]\,dz \quad (2b)$$

and

$$g(z) = \sum_{n=0}^{\infty} b_n \sin[(2n+1)\pi z/2c] \quad (3a)$$

$$b_n = \frac{1}{c}\int_{-c}^{+c} g(z)\sin[(2n+1)\pi z/2c]\,dz \quad (3b)$$

Now, because $(\sigma_{rr})_{r=a} = \mu f(z)$ and $(\sigma_{rz})_{r=a} = \mu g(z)$, these can be compared with the general equations whose derivation is outlined in Appendix A. The result is the following set of equations:

$$\frac{\sigma_{rr}}{\mu} = \sum\left\{-[(1+\gamma)A_1 + (1-\gamma)A_2]I_0(\rho) + 2\left(\frac{A_1}{\rho} - \frac{C}{k}\rho\right)I_1(\rho)\right\}\cos(kz) \quad (4a)$$

$$\frac{\sigma_{\phi\phi}}{\mu} = \sum\left[-\frac{2A_1}{\rho}I_1(\rho) - \frac{(1-\gamma)}{\gamma}\frac{2C}{k}I_0(\rho)\right] \times \cos(kz) \quad (4b)$$

$$\frac{\sigma_{zz}}{\mu} = \sum\left\{[2\gamma+1)A_2 - (2\gamma-1)A_1]I_0(\rho) + \frac{2C}{k}\rho I_1(\rho)\right\}\cos(kz) \quad (4c)$$

$$\frac{\sigma_{rz}}{\mu} = \sum\left[(A_1 + A_2)I_1(\rho) + \frac{2C}{k}\rho I_0(\rho)\right] \times \sin(kz) \quad (4d)$$

$$u = -\sum\left[A_1 I_1(\rho) + \frac{C}{k}\rho I_0(\rho)\right] \times \frac{\cos(kz)}{k} \quad (4e)$$

$$w = \sum\left[A_2 I_0(\rho) + \frac{C}{k}\rho I_1(\rho)\right] \times \frac{\sin(kz)}{k} \quad (4f)$$

where $\gamma = (\lambda + \mu)/\lambda + 2\mu)$ and $\rho = kr$. Noting that $\nu = \lambda/2(\lambda - \mu)$, then a simple derivation shows γ to be given by $1/2(1 - \nu)$. In this way the effects of different Poisson ratios can be assessed. The constants A_1, A_2 and C are found by substituting the Fourier coefficients calculated from Equations 2 and 3 into

$$A_1 = -\frac{a_n[\alpha I_1(\alpha) + \gamma\alpha^2 I_0(\alpha)] + b_n[\gamma\alpha^2 I_1(\alpha) + (1-\gamma)\alpha I_0(\alpha)]}{2[\gamma\alpha^2 I_0^2(\alpha) - (1+\gamma\alpha^2)I_1^2(\alpha)]} \quad (5)$$

$$A_2 = -\frac{a_n[\alpha I_1(\alpha) + \gamma\alpha^2 I_0(\alpha)] + b_n[(1+\gamma)\alpha I_0(\alpha) - (2+\gamma\alpha^2)I_1(\alpha)]}{2[\gamma\alpha^2 I_0^2(\alpha) - (1+\gamma\alpha^2)I_1^2(\alpha)]} \quad (6)$$

$$C = \frac{(2n+1)\pi}{2c}\frac{a_n\alpha\gamma I_1(\alpha) + b_n[\gamma\alpha I_0(\alpha) - \gamma I_1(\alpha)]}{2[\gamma\alpha^2 I_0^2(\alpha) - (1+\gamma\alpha^2)I_1^2(\alpha)]} \quad (7)$$

To enable the implementation of these equations on a computer, r and z are allowed to assume only discrete values and the stresses and displacements are therefore calculated on a mesh throughout the fibre. If the radius is divided into m divisions and the half-length into p divisions, then the values of r become $r_i = ia/m$ $(i = 0, 1 \ldots, m)$ and of z are $z_j = jc/p$ $(j = 0, 1 \ldots, p)$. The ratio of the length to the diameter of the fibre, the axial ratio, is denoted by $q(= c/a)$. Iterations are therefore set up to step through all the values of i and j and calculate the displacements u and w and the stresses σ_{rr}, σ_{rz}, σ_{zz} and $\sigma_{\varphi\varphi}$ for given values of q and τ where $\tau = (\sigma_{rz})_{r=a}$. The Bessel's functions are calculated from their series expansions [12]. The radial contraction, u, and the longitudinal extension, w, are calculated as multiples of $\tau a/\mu$. Similarly the stresses are calculated as multiples of τ alone and, therefore, scale directly as the magnitude of the stress transferred to the fibre from the matrix.

3. Applications

The systems considered will be those that have only an applied shear stress over the curved surface. So,

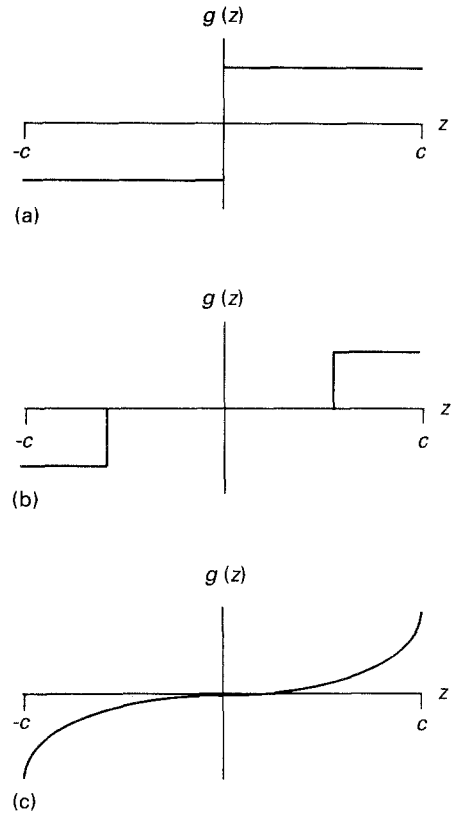

Figure 1 Schematic plots of stress-transfer functions considered in the analysis.

$\sigma_{rr} = 0$ at $r = a$ and $\sigma_{zz} = 0$ at $z = \pm c$, and it is readily seen that $u_0 = w_0 = 0$ and $a_n = 0$. The coefficients b_n will be calculated from the Fourier series for each form of $g(z)$ considered for σ_{rz}. Three forms for this stress-transfer function will be considered and these are illustrated in Fig. 1. These are constant shear over the whole fibre length, constant shear over a fraction of the fibre near the ends and finally the shear-lag distribution [2] described by a hyperbolic sine function.

3.1. Constant shear stress

The simplest case to treat first is one of constant stress transfer along the whole length of the fibre. This will serve to illustrate the sort of results to be expected from a metallic or plastically deforming matrix which applies a constant stress over the surface of the fibre.

The stress transfer function, $g(z)$, is given by $\mu g(z) = \tau$ for $0 \leqslant z \leqslant c$ and $\mu g(z) = -\tau$ for $-c \leqslant z < 0$ and the Fourier coefficients b_n are given by

$$b_n = 4\tau/\mu(2n + 1)\pi \qquad (8)$$

Substitution of Equation 8 into Equation 4a–f yields values for the constants A_1, A_2 and C as described in Equations 5–7. Three values of axial ratio were analysed: $q = 10$, 100 and 1000 each with two values of Poisson ratio, $\nu = 0.25$ and 0.4.

Fig. 2 shows the variation of axial stress, σ_{zz}, along the fibre for fibres with large axial ratios. It shows a linear increase from the end of the fibre to the centre where it reaches a value of $2q\tau$, independent of ν. For small q the distribution is very similar except that it overshoots at the midpoint of the fibre on the surface, by more than 15%, and there is therefore a significant difference between the axial stress along the centre of the fibre and that at the outer surface. This is due, at least in part, to the artificial loading pattern, which has a discontinuity at the fibre midpoint, and to the slow convergence of some of the series at the boundaries of the problem.

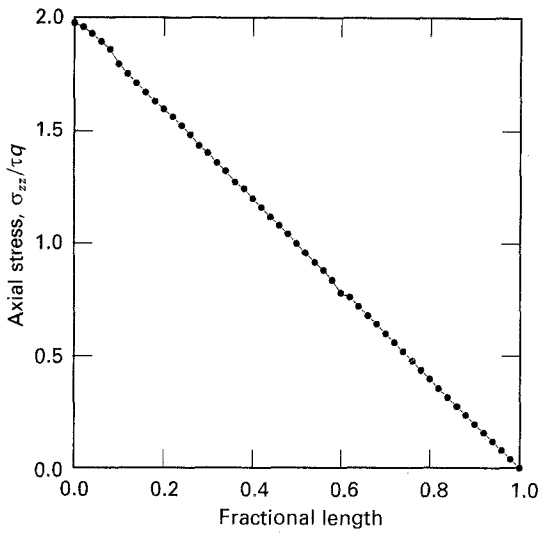

Figure 2 Variation of axial stress, σ_{zz}, along the length of a fibre for a constant shear stress transfer, τ, as shown in Fig. 1a. The results are scaled by the axial ratio q to enable them to be superimposed.

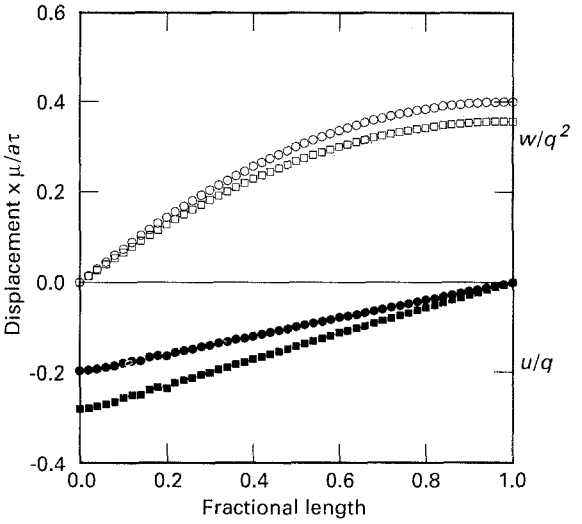

Figure 3 Variation of lateral displacement, u, and axial displacement, w, along the length of the fibre for a constant shear stress transfer, τ, as shown in Fig. 1a. These can be superimposed for all fibre lengths if scaled by q and q^2, respectively, as described in the text. (○, ●) $\nu = 0.25$, (□, ■) $\nu = 0.4$.

The axial and radial displacements are shown in Fig. 3. The radial displacement, u, is calculated as a non-dimensional multiplier of $a\tau/\mu$ and is shown normalized by the axial ratio as this allows all the results to be superimposed. As the radial strain is homogeneous it is defined by the displacement divided by the radius. So, to calculate the radial strain from the graph it is therefore necessary to multiply the result shown by $q\tau/\mu$. It can be seen that the value for

the Poisson's ratio makes a significant difference to both the radial and axial strains. The radial strain is compressive, decreases along the length of the fibre and increases with the Poisson's ratio. In contrast, the axial strain is not homogeneous, being given by the gradient of the displacement curve in Fig. 3. It is greatest at the midpoint of the fibre and decreases linearly to zero at the ends. The magnitude of this strain decreases with increasing Poisson's ratio. The calculated values for axial displacement, w, are again dimensionless multipliers of $a\tau/\mu$. To express this in terms of fibre length, rather than radius, multiply numerator and denominator of this expression by q to change w to a multiplier of $c\tau/\mu q$. This scales with q in the same way as did the radial strain, and so the graph for w is shown normalized by q^2. Only in fibres with a small axial ratio was there any significant variation in axial stress or strain across the radius of the fibre. At the surface both of these were about 14% higher than along the z-axis. (The surface stress will actually have a discontinuity at $z = 0$ due to the form of function chosen for $g(z)$). The effect of these strain gradients will be to distort the planarity of the fibre ends which may, in practice, affect fibre-end bonding. However, this will not be considered here.

3.2. Constant shear stress at fibre ends

If a constant shear stress is applied to the fibre surface over a fraction of the fibre at the ends then the more traditional description of fibre axial stress appears. This stress distribution could arise, as before, from plastic flow of the matrix over the fibre or by friction between the fibre surface and the matrix, but in this case be ineffective at the centre of the fibre due to the smaller relative movement of fibre and matrix. This distribution is somewhat contrived but is the only one that gives results that are similar to textbook illustrations. Fig. 4 shows that the axial stress rises linearly over the part of the fibre subject to the applied shear,

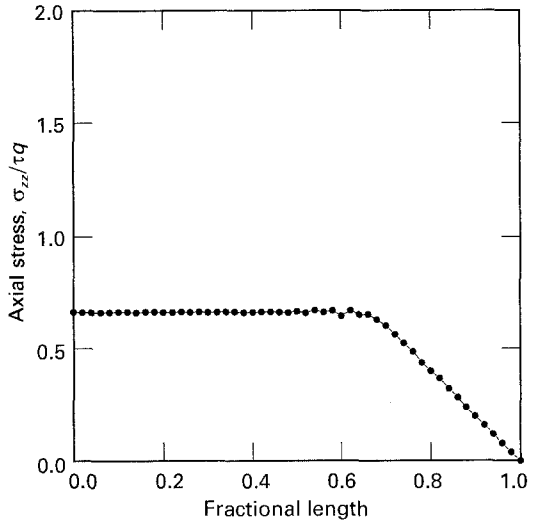

Figure 4 Variation of axial stress, σ_{zz}, along the length of a fibre for a constant shear stress transfer, τ, over the terminal one-third of the fibre as shown in Fig. 1b. The results are scaled by the axial ratio q to enable them to be superimposed.

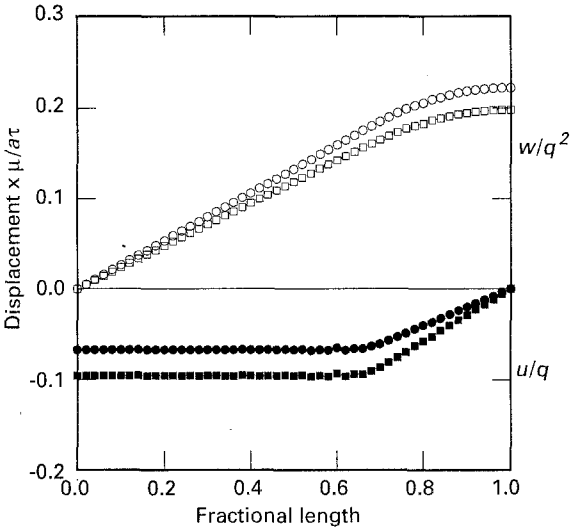

Figure 5 Variation of lateral displacement, u, and axial displacement, w, along the length of the fibre for a constant shear stress transfer, τ, over the terminal one-third of the fibre as shown in Fig. 1b, These can be superimposed for all fibre lengths if scaled by q and q^2, respectively, as described in the text. (○, ●) $\nu = 0.25$, (□, ■) $\nu = 0.4$.

in this case the terminal one-third. Over the remainder of the fibre it remains constant with a value of $2ql_f/\tau$ where l_f is the fraction of the fibre length over which the shear stress is applied. It is now the combination of the axial ratio and the fraction of the fibre over which stress is transferred that determine the fibre stress for a given applied shear stress.

The strains in the fibre will be similarly altered from the continuous case described above. Fig. 5 shows the radial and axial displacements in a fibre in which stress is transferred over one-third of the fibre length. The axial ratio, q, again serves as a normalizing factor that enables the results for all fibre lengths to be superimposed. The compressive radial strain may be calculated by multiplying the displacement shown, u/q, by $q\tau/\mu$ as before. Similarly to the axial stress, the radial strain scales from that found for continuous stress transfer by the factor of the fractional length of the stress transfer region. So, in the case plotted in Fig. 5, the maximum displacement is one-third that found for the continuous transfer. The axial strain is constant over the central part of the fibre, again with a magnitude reduced by the factor l_f and decreases linearly to the fibre end where it is zero. It may also be calculated by similar methods to those outlined above.

3.3. Shear-lag

The standard analysis for elastic stress transfer caused by the different strains generated in fibre and matrix due to their different moduli is due to Cox [2]. This is treated comprehensively in several books [3, 8, 9] though, once again, there are inconsistencies. The analytical method involves first calculating the axial stress in the fibre then deriving the stress transfer function applied to the surface. The treatment here is slightly different to previous ones in that the origin is chosen to be at the mid-point of the fibre, as this simplifies the

mathematics, and the stress transfer function is assumed to be that derived from the shear-lag analysis. The stress and strains in the fibre are then calculated for all r and z.

The standard analytical result for the axial stress is given by

$$\sigma_f = E_f \varepsilon_f \left(1 - \frac{\cosh(\beta z)}{\cosh(\beta c)}\right) \quad (9)$$

where

$$\beta = \left[\frac{2G_m}{E_f a^2 \ln(R/a)}\right]^{1/2} \quad (10)$$

which may be written as $\beta = \beta'/a$ and β' is now dimensionless. Nomenclature is as before and, in addition, G_m is the shear modulus of the matrix, E_f the fibre modulus, ε the strain in the composite and $2R$ the mean spacing of the fibres normal to their length. The shear stress along the surface of the fibre is then given by

$$\tau = E_f \varepsilon \left[\frac{G_m}{2E_f \ln(R/a)}\right]^{1/2} \frac{\sinh(\beta z)}{\cosh(\beta c)} \quad (11)$$

which may be written

$$\tau = \tau_0 \frac{\sinh(\beta z)}{\cosh(\beta c)} \quad (12)$$

If $g(z) = \sinh(\beta z)/\cosh(\beta c)$ then from Equation 3 the Fourier coefficients are given by

$$b_n = \frac{(-1)^n 2\beta}{c(\beta^2 + k^2)} = \frac{(-1)^n 8\beta'}{(4q^2\beta'^2 + k'^2)} \quad (13)$$

where $k = (2n + 1)\pi/2c = k'/2c$. Inserting these into Equations 4–7 gives the required results. For the purposes of calculation, values were assigned to the ratio of matrix shear modulus to fibre modulus of 4×10^{-3} and 10^{-1} as these are the figures that correspond to sapphire fibres in a resin and a metal, respectively ([3], p. 262). The logarithmic packing function is slowly varying, for instance for R/a in the range 2–20 the logarithm only increases from 1 to 3. A value of 2 was chosen for ease of comparing figures but the dependency of the results on this parameter could also be investigated separately. This means that $\beta' = (G_m/E_f)^{1/2}$. It also needs to be noted that there is an implicit dependency on the aspect ratio, q, in the argument of the hyperbolic functions above; βz may be written $\beta' qz/c$ and βc becomes $\beta' q$.

Fig. 6 shows the shear stress, σ_{rz}, for various values of $q\beta'$ along the half-fibre. For small values of $q\beta'$ the increase in stress from zero at the centre towards the fibre ends is essentially linear, because $\sinh(x) \sim x$ and $\cosh(x) \sim 1$ for small x. Increasing the value of G_m and therefore β' has the same effect as increasing the aspect ratio of the fibre, and it can be seen that stress is transferred over smaller fractions of the fibre length concentrated at the ends. The consequence is that the fibre is fully stressed along a greater proportion of its

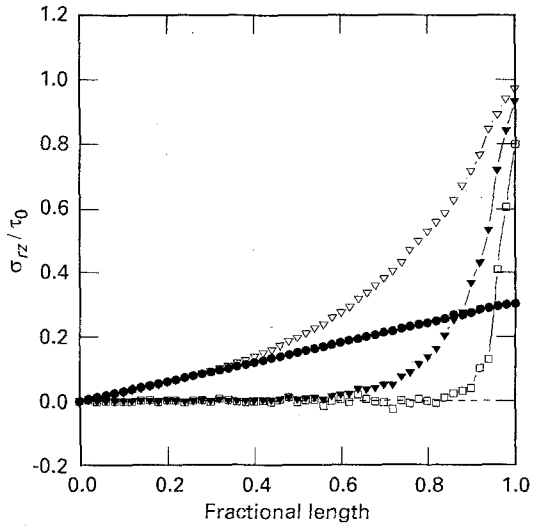

Figure 6 Variation of shear stress, σ_{rz} along the outer surface of the fibre for the values of $q\beta'$ shown, assuming a shear-lag form of stress transfer as shown in Fig. 1c. As the axial ratio increases, stress is transferred over increasingly smaller fractions of the fibre at the fibre ends. $q\beta'$:(●) 0.01, (▽) 0.1, (▼) 1.0, (□) 10.0.

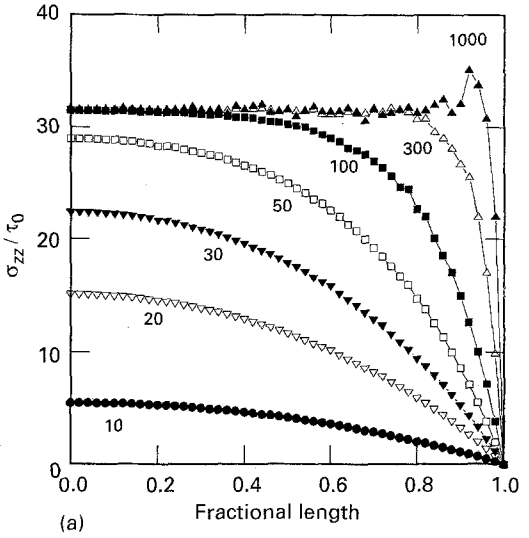

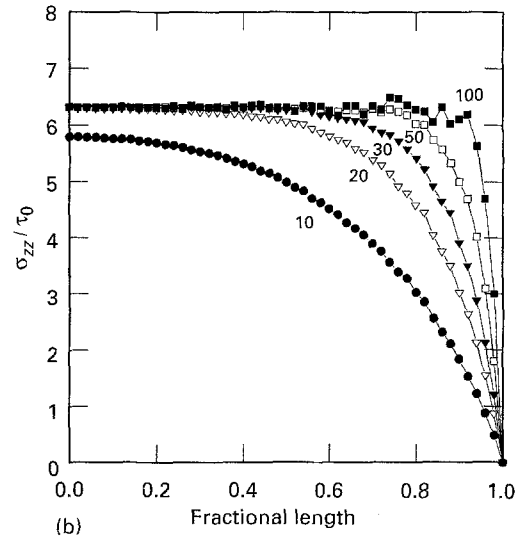

Figure 7 Axial stress generated along the fibre length for (a) $G_m/E_f = 0.004$ and (b) $G_m/E_f = 0.1$ assuming a shear-lag form of stress transfer as shown in Fig. 1c. As the axial ratio, q, increases, as shown, an increasing fraction of the fibre becomes maximally stressed.

length, as shown in Fig. 7. However, Fig. 7 also shows that in terms of the maximum axial stress in the fibre, the effects of increasing G_m are not the same as increasing the fibre length. By equating the axial force generated in the fibre at a given position with the shear stress transferred up to that position (Appendix B) it may be shown that the peak axial stress at the centre of the fibre $(\sigma_{zz}/\tau_0)_{max} = 2/\beta'$ providing the fibre is long enough for the sinh function for σ_{rz} to have fallen to almost zero. If, once again, the logarithmic term is removed, then the peak stress becomes $2(E_f/G_m)^{1/2}$ and this may be seen in Fig. 7 for the two values of G_m/E_f (4×10^{-3} and 0.1) plotted. Almost paradoxically, the peak axial fibre stress increases as the matrix shear modulus decreases for a given fibre modulus. As the fibre axial ratio increases the axial stress along the fibre first increases monotonically along the whole length of the fibre until the fibre is sufficiently long that the peak stress, described above, occurs. After this

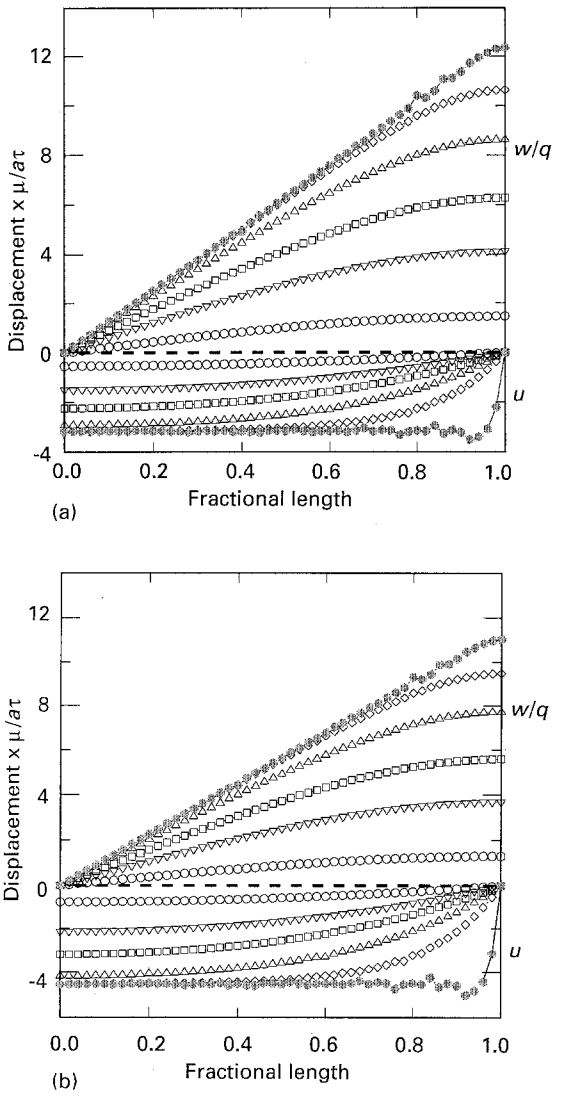

Figure 8 Variation of lateral displacement, u, and axial displacement, w, along the length of the fibre for a shear-lag form of stress transfer to the fibre, as shown in Fig. 1c, with $G_m/E_f = 4 \times 10^{-3}$. The effects of increasing the Poisson's ratio from (a) $\nu = 0.25$, to (b) $\nu = 0.4$ are shown. The lateral displacements converge as q increases, so these can be plotted on the same axes for all fibre lengths, as can w if scaled by q as described in the text. q:(○) 10, (▽) 20, (□) 30, (△) 50, (◇) 100, (●) 1000.

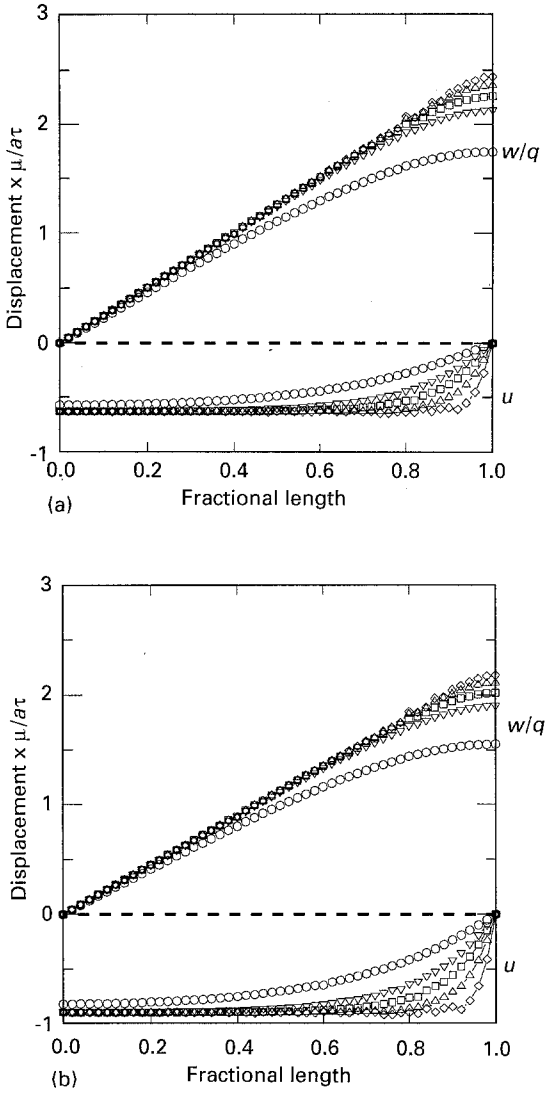

Figure 9 Variation of lateral displacement, u, and axial displacement, w, along the length of the fibre for a shear-lag form of stress transfer to the fibre, as shown in Fig. 1c, with $G_m/E_f = 0.1$. The effects of increasing the Poisson's ratio from (a) $\nu = 0.25$, to (b) $\nu = 0.4$ are shown. The lateral displacements converge as q increases, so these can be plotted on the same axes for all fibre lengths, as can w if scaled by a as described in the text. q:(○) 10, (▽) 20, (□) 30, (△) 50, (◇) 100.

is reached the stress cannot increase further for a given applied stress but the plateau region of maximum stress extends further along the length of the fibre. This is seen most clearly for the weakly interacting system in Fig. 7a. It may be seen that the maximum fibre stress scales directly with the magnitude of the applied shear stress. However, increasing the applied shear stress does not change the length of the maximally stressed plateau region. This result is confirmed by experimental measurements [5] which show no change, provided there is no debonding between fibre and matrix. This again contrasts with common portrayals, e.g. [8], which show the plateau region diminishing as the applied stress increases until the fibre breaking stress is reached.

The displacements generated in the fibre by the above stresses are shown in Figs 8 and 9. The axial displacements are scaled by the axial ratio so that they can be plotted on the same axes but the radial ones

converge and do not require scaling. However, there is now a clear dependency of these parameters on the axial ratio not just in magnitude as before but also in the form of the distribution. These appear to follow the stress patterns shown in Figs 6 and 7 and are dependent on the Poisson's ratio of the fibre material. Only for fibres of very small values of $q\beta'$ is there any significant difference in the stresses or the strains at the surface compared with those along the axis $r = 0$. This difference was about 4% for the axial stress and strain for fibres of $q = 10$ and $G_m/E_f = 4 \times 10^{-3}$.

4. Critical length

From these analyses there are a number of ways of introducing a critical length, based on fibre failure, or a stress-transfer length relying on the requirement to transfer effectively as much stress as possible to the fibre. For the first case considered, the analysis clearly demonstrates that if the stress transfer to the surface of the fibre is assumed to act along the whole length of the fibre and not just at the ends, no plateau is developed in the axial stress; it rises constantly to its maximum value at the midpoint of the fibre. For a given value of τ, the critical axial ratio, q_c, which is such as to allow this stress to reach the breaking stress of the fibre, $\sigma_{zz} = \sigma_f^*$, is given by

$$\sigma_f^* = 2q_c\tau \tag{14}$$

This is easily rearranged to give the classical expression for the so-called critical length, $l_c = a\sigma_f^*/\tau$. However, this does not correspond to a stress-transfer length, as stress is applied along the whole length of the fibre. The commonly shown diagram of stress rising over this critical length at the ends of the fibres and then remaining constant over the central region cannot be realized with this form of stress transfer.

If the stress is only applied over a fraction of the fibre at the ends, then the above expression is modified so that the maximum fibre stress will reach the fracture stress if

$$\sigma_f^* = 2q_c l_f \tau \tag{15}$$

In this case, the critical axial ratio for a given value of τ will increase as the stress-transfer fractional length decreases from the full length of the fibre considered above. In this case there is a plateau in the axial stress corresponding to the unloaded part of the fibre. However, the length of this plateau does not decrease as the magnitude of the shear stress increases, it remains a constant fraction of the fibre length. So, if the axial stress approaches the fracture strength of the fibre it will do so over the whole of this length and failure can therefore occur at any point.

For the case of a shear-lag stress transfer function defined by Equation 12, the maximum value of τ occurs when $z = c$ and so $\tau = \tau_0 \tanh(\beta' q)$. Now $\tanh(x) \to 1$ as $x \to \infty$ and so, for instance, τ rises to within 1% of its theoretical maximum when $\tanh(q\beta') = 0.99$, i.e. $q\beta' = 2.7$. If this is used to define a critical stress transfer length, q_c, then

$$q_c = 2.7/\beta' \approx 2.7(E_f/G_m)^{1/2} \tag{16}$$

This definition now has nothing to do with fracture of the fibre, but dictates what length of fibre is required for the shear stress to be able to rise to within some previously determined fraction of its theoretical maximum at the fibre ends. If this value of $\beta' q$ is substituted into Equation 8 and the value of the axial stress determined at the fibre centre, $z = 0$, then it is readily shown that the fibre stress is about 13% lower than the theoretical maximum. This is illustrated in Fig. 7a where if $\beta'^2 = G_m/E_f = 4 \times 10^{-3}$ then the critical stress-transfer length is $q_c = 2.7/\beta' = 43$ and the predicted value of the axial stress at $z = 0$ is $(0.87) \times 2/\beta' = 27$. Interpolating the curves shown for various values of q shows that this is indeed the case. However, it is clear from the same figure (Fig. 7a) that the axial stress does not appear to reach its maximum until $q \sim 100$. Another definition of q could, therefore, be derived from Equation 8 as the axial ratio for which the axial stress reaches within 1% of its theoretical maximum. Appendix B derives an expression for the maximum axial stress, and from Equation A10, by requiring that $\text{sech}(\beta' q) = 0.01$ leads to the value $q_c = 5.3/\beta' = 83$. Once again this has no immediate connection with fibre failure but is derived from a consideration of maximum utilization of the fibre properties. However, to find the smallest value of q for which the maximum axial stress can reach the breaking stress then again from Equation A10 $\sigma_f^* = 2\tau_0/\beta'$. Substituting for β' from the above expression for q_c leads to $q_c = 5.3\sigma_f^*/2\tau_0$. All the above analyses have thus shown that a critical stress-transfer length can be defined as some multiple of $1/\beta'$, $q_c = Q_m/\beta'$, and so $q_c = Q_m(\sigma_f^*/2\tau_0)$. This is very similar to the commonly accepted definition as derived for the constant stress-transfer case with exception of the multiplier, which has been shown to be hard to define precisely. Could this be a source of the discrepancy sometimes noted [8] that measured stress-transfer appears to be greater than predicted by these simple models? If Q_m is assumed to be 1, then more stress would have to be transferred over that distance than if Q_m is allowed to be some larger figure.

5. Conclusion

A method is presented for calculating stresses and strains within a fibre in a fibre–composite material from an assumed surface distribution of shear stress by expressing solutions as a series of harmonic terms. End adhesion is ignored at this stage. The results show that care needs to taken when describing patterns of stress transfer and definitions of so-called critical lengths. The salient results of this analysis, common to all patterns of stress transfer considered, are that (i) axial fibre stress scales in direct proportion to the magnitude of the applied shear stress, and (ii) when, by the nature of the stress transfer function, a plateau region occurs in the axial stress, its length is independent of the applied stress. In addition, for elastic matrices in which the shear-lag description of stress transfer is used the stress-transfer length is longer than given by the simple formula by a multiple that depends on the criterion chosen for defining optimum

stress transfer. The analysis can be extended in future to include adhesion at the fibre ends and the effects of different Poisson's ratios in the fibre and matrix, which would lead to either radial compressive or tensile forces over the cylindrical fibre surface. Some consequences that could be examined are the change in planarity of the fibre ends and stress and strain gradients generated within the fibre that could lead to failure.

Acknowledgements

The author thanks Dr D. W. L. Hukins for valued criticism of early drafts of the manuscript, and the Medical Research Council and Action Research for their financial support.

Appendix A

The starting point of the derivation is the following set of equations

$$(\lambda + 2\mu)\frac{d^2u}{dr^2} + (\lambda + 2\mu)\frac{d}{dr}\left(\frac{u}{r}\right) + \mu\frac{d^2u}{dz^2} + (\lambda + \mu)\frac{d^2w}{drdz} = 0 \quad \text{(A1)}$$

$$\frac{d}{dr}\left[\frac{1}{r}\frac{d(rv)}{dr}\right] + \frac{d^2v}{dz^2} = 0 \quad \text{(A2)}$$

$$(\lambda + \mu)\left(\frac{d^2u}{drdz} + \frac{1}{r}\frac{du}{dz}\right) + \mu\left(\frac{d^2w}{dr^2} + \frac{1}{r}\frac{dw}{dr}\right) + (\lambda + 2\mu)\frac{d^2w}{dz^2} = 0 \quad \text{(A3)}$$

$$\sigma_{rr} = (\lambda + 2\mu)\frac{du}{dr} + \lambda\frac{u}{r} + \lambda\frac{dw}{dz}$$

$$\sigma_{rz} = \mu\left(\frac{dw}{dr} + \frac{du}{dz}\right)$$

$$\sigma_{zz} = \lambda\left(\frac{du}{dr} + \frac{u}{r}\right) + (\lambda + 2\mu)\frac{dw}{dz}$$

$$\sigma_{\phi z} = \mu\frac{dv}{dz}$$

$$\sigma_{\phi\phi} = (\lambda + 2\mu)\frac{u}{r} + \lambda\frac{du}{dr} + \lambda\frac{dw}{dz}$$

$$\sigma_{r\phi} = \mu\left(\frac{dv}{dr} - \frac{v}{r}\right) \quad \text{(A4)}$$

Equation 1 is derived by differentiating Equation A1 with respect to r and Equation A3 with respect to z and then eliminating either du/dz or dw/dr between the results.

Solutions to Equation 1 are found in a similar way to solutions to Laplace's equation. Care needs to be taken to find all the solutions, as Equation 1 is fourth-order whereas Laplace's equation is only second-order. Filon finds the possible sets of product functions satisfying Equation 1 to be

$$\begin{aligned} y = {} & A\cos(kz + \alpha)I_1(kr) \\ & B\cos(kz + \beta)K_1(kr) \\ & C\cos(kz + \gamma)rI_0(kr) \\ & D\cos(kz + \delta)rK_0(kr) \\ & Ez\cos(kz + \varepsilon)I_1(kr) \\ & Fz\cos(kz + \theta)K_1(kr) \end{aligned} \quad \text{(A5)}$$

where $k = (2n + 1)\pi/2c$ and I and K are hyperbolic (or modified) Bessel functions of the first and second kinds.

The solutions for a circular cylinder under the system of stresses described above are composed of a series of terms of the form above but only containing the I functions.

$$\begin{aligned} \frac{du}{dz} = {} & \sum[A_1\cos(kz + \alpha_1)I_1(kr) \\ & + C_1\cos(kz + \gamma_1)rI_0(kr) \\ & + E_1z\cos(kz + \varepsilon_1)I_1(kr)] \end{aligned} \quad \text{(A6)}$$

$$\begin{aligned} \frac{dw}{dr} = {} & \sum[A_2\cos(kz + \alpha_2)I_1(kr) \\ & + C_2\cos(kz + \gamma_2)rI_0(kr) \\ & + E_2z\cos(kz + \varepsilon_2)I_1(kr)] \end{aligned} \quad \text{(A7)}$$

The K functions are not used in this case as they lead to infinite terms at the axis. Integrating and putting in boundary conditions leads to expressions for u and w which can be substituted back into Equations A1 and A3. This leads ultimately to a set of equations for the displacements u and w and the stresses σ_{rr}, σ_{zz} and σ_{rz}. By considering the surface of the cylinder, $r = a$, and comparing the Fourier series expansions of the applied stresses with those calculated here, expressions can be found for the stresses and strains in the particular case of interest. These are given in the text without further derivation and are the ones implemented for this study. The full treatment is provided by Filon [11].

Appendix B

Analysis of the shear-stress transfer equations can give some further insight into the behaviour of this system and provide a check on the answers given by the computer model. The axial force produced at the central plane of the fibre, $z = 0$, can be equated to the total shear stress transferred over the curved surface

$$\pi a^2(\sigma_{zz})_z = -2\pi a\int_c^z (\sigma_{rz})_{r=a}\,dz \quad \text{(A8)}$$

Using

$$(\sigma_{rz})_{r=a} = \tau_0\sinh(\beta' z/a)/\cosh(\beta' q) \quad \text{(A9)}$$

from Equation (12), and noting that the maximum value of σ_{zz} is at $z = 0$ then solving equation A8

$$(\sigma_{zz})_{z=0} = (2\tau_0/\beta')[1 - \operatorname{sech}(\beta' q)] \quad \text{(A10)}$$

Now $\operatorname{sech}(x) \to 0$ as $x \to \infty$ so that for large $q\beta'$

$$\frac{(\sigma_{zz})_0}{\tau_0} = \frac{2}{\beta'} = 2\left[\frac{E_f}{G_m}\frac{\ln(R/a)}{2}\right]^{1/2} \quad \text{(A11)}$$

Putting $\ln(R/a) = 2$ as described previously and with

$(G_m/E_f) = 4 \times 10^{-3}$, leads to $(\sigma_{zz})_0/\tau_0 = 31$ as shown in Fig. 7.

References

1. R. M. ASPDEN, *Proc. R. Soc. Lond.* **A406** (1986) 287.
2. H. L. COX, *Br. J. Appl. Phys.* **3** (1952) 72.
3. A. KELLY and N. H. MACMILLAN, "Strong Solids", 3rd Edn (Oxford University Press, Oxford, 1986).
4. Y. TERMONIA, *J. Mater. Sci.* **22** (1987) 504.
5. C. GALIOTIS, R. J. YOUNG, P. H. J. YEUNG and D. N. BATCHELDER, *ibid.* **19** (1984) 3640.
6. I. M. ROBINSON, R. J. YOUNG, C. GALIOTIS and D. N. BATCHELDER, *ibid.* **22** (1987) 3642.
7. E. M. ASLOUN, M. NARDIN and J. SCHULTZ, *J. Mater. Sci.* **24** (1989) 1835.
8. D. HULL, "An introduction to composite materials", (Cambridge University Press, Cambridge, 1981).
9. G. S. HOLISTER and C. THOMAS, "Fibre Reinforced Materials" (Elsevier, Barking, UK, 1966).
10. S. P. TIMOSHENKO and J. N. GOODIER, "Theory of Elasticity", 3rd Edn (McGraw-Hill, Singapore, 1970).
11. L. N. G. FILON, *Phil. Trans. R. Soc. Lond.* **A198** (1902) 147.
12. G. N. WATSON, "Treatise on the theory of Bessel functions", (Cambridge University Press, Cambridge, 1922).

Received 30 March
and accepted 8 June 1993